Quasi-one-dimensional phosphorene nanoribbons grown on silicon by space-confined chemical vapor transport

Kaixiang Du,[1,‖] Mingyuan Wang,[2,‖] Zhiping Liang,[1] Quanjiang Lv,[1] Haigang Hou,[1]

Shuangying Lei,[2] Shahid Hussain,[1] Guiwu Liu,[1,a] Junlin Liu,[1,a] Guanjun Qiao[1,a]

AFFILIATIONS

1School of Materials Science and Engineering, Jiangsu University, Zhenjiang 212013, China

2SEU-FEI Nano-Pico Center, Key Laboratory of MEMS of Ministry of Education, School of Electrical Science and Engineering, Southeast University, 210096 Nanjing, China

a)Authors to whom correspondence should be addressed: gwliu76@ujs.edu.cn, gjqiao@ujs.edu.cn, and liujunlin@ujs.edu.cn

‖ These authors contributed equally.
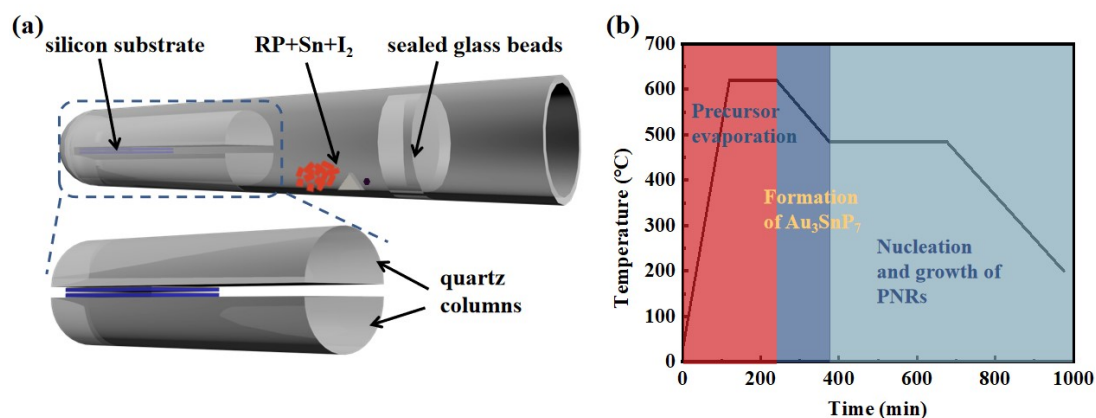
Samples fabrication process

FIG. S1. (a) Schematic of experimental setup: Two semi-circular quartz columns and two silicon substrates are placed inside the quartz ampule tube; (b) Temperature profile of the employed growth process.

Before PNRs growth, the Au film (~100 nm) was deposited on the silicon substrate by thermal evaporation deposition. Two semi-cylindrical quartz columns were set in the ampules. The silicon substrate was placed between two semicircular quartz columns to form a space-confined system. Red phosphorus (50~200 mg, Alfa Aesar, 99.999% metal basis), tin (3~12 mg, Aladdin, powder, 99.99% trace metal basis), and iodide (1.5~5 mg, Alfa Aesar, 99.999% trace metal basis) are the source materials for the PNRs growth [Fig. S1(a)]. The materials together with a space-confined system were transferred sequentially into a quartz ampule (inner diameter 1.6 cm and length 17 cm) in a glove box. After removing the ampule from the glove box, using a vacuum pump device, the ampule was evacuated down to 10^{-3} Pa. Subsequently, the ampule was sealed via an oxy-hydrogen sealing machine. The ampule was placed in

the muffle furnace to start the PNRs growth. Temperature profile of the employed temperature-controlled growth process is shown in Fig. S1(b). The furnace was heated to 620 °C slowly. After that, it was held at 620 °C for 2 h, and then cooled down to 485 °C slowly, and held at the temperature for another 5 h. Then, the temperature was decreased to 200 °C slowly, and finally to room temperature naturally.

Materials characterization

The microstructure of the PNRs samples was characterized by the scanning electron microscope (SEM: FEI Nova Nano 450) combined with energy dispersive X-ray spectrometry (EDS). Their detailed nano structures were characterized via high-resolution transmission electron microscopy (HRTEM: FEI Talos F200s) and selected area electron diffraction (SAED) pattern to study the morphologies and chemical compositions. A Priston CCD Raman Microprobe (DL-2 Instruments) provides insight into all sp^3-bonded P allotropes. The X-ray diffraction (XRD, D8 Advance, Bruke) patterns of PNRs samples were characterized with Cu-Kα radiation at 40 kV and 30 mA in the 2θ range of 10-90°. The valences of P element were analyzed by employing X-ray photoelectron spectra (XPS: AXIS SUPRA).

Calculation Method. In this work, the calculations were performed by density functional theory (DFT) based on the Vienna Ab initio Simulation Package (VASP).[1,2] The GGA and PBE functionals were applied for describing electron correlation.[3] The ion-electron interaction is described by using the projector augmented wave (PAW) method.[4] A vacuum space exceeding 15 Å in the z-direction was employed to avoid the interaction between two periodic layers and the van der Waals (vdW) interactions were taken into consideration using DFT-D3.[5] A cutoff energy of 400 eV was set and the Brillouin Zone was chosen as 3×3×1 grid, and the convergence criteria of energy and force were set as 10^{-5} eV per atom and 0.02 eV/Å, respectively. The adsorption energy (ΔE) was calculated by following equation:[6,7]

$$\Delta E = E_{total} - E_{BP} - E_{P4}$$

Eq. S1

where E_{total}, E_{BP} and E_{P4} are the total energies for the P_4 molecules adsorbed on phosphorene, the substrate slab phosphorene and the P_4 molecules, respectively. The energy barriers of transition states for the understanding the growth of phosphorene were determined using a climbing image nudged elastic band (CINEB) method.[8] The energy barriers of transition states for the understanding the growth of phosphorene were calculated using a climbing image nudged elastic band (CINEB) method. Additionally, to keep the CINEB results consistent with structure optimization, the same convergence criteria were set, and 4 points are inserted in CINEB calculation.
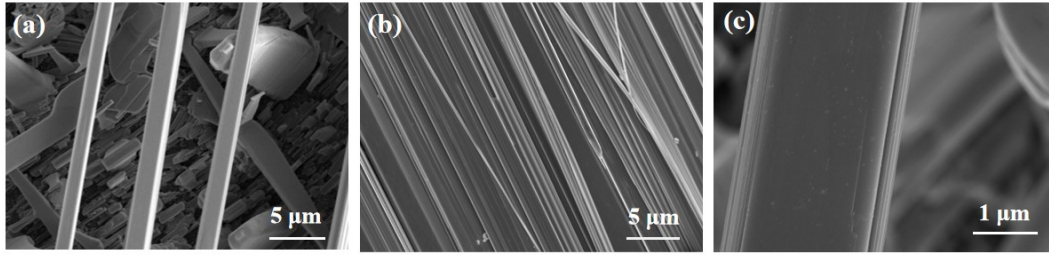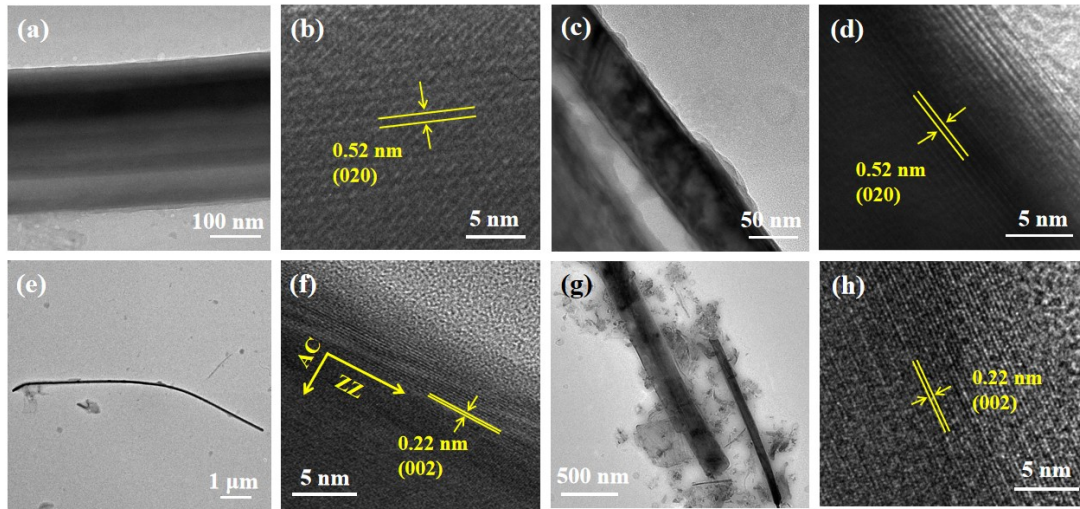
FIG. S2. SEM images of PNRs

FIG. S3. TEM and HRTEM images of PNRs in different regions, indicating (a-d) the thicknesses of PNRs and the lattice spacing of 0.52 nm corresponding to (020) plane, and (e-h) the widths of PNRs and lattice spacing of 0.22 nm corresponding to (002) plane.
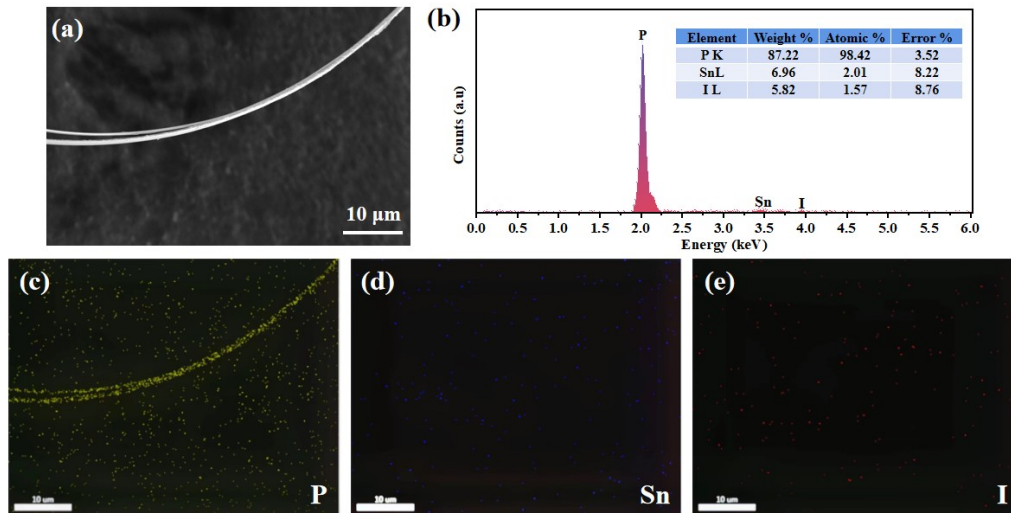
FIG. S4. EDS analysis of PNRs on the silicon substrate: (a) SEM image of PNRs; EDS spectrum and elemental composition; The corresponding element mapping of (c) P, (d) Sn, and (e) I.

In the growing process, Au reacted with P and Sn to form the distributed Au_3SnP_7 on silicon, which plays the critical role of nucleation of BP. Meanwhile, Sn reacted with I_2 to form the SnI_4, which acts as the mineralizer to promote the reaction. This can eliminate the catalysts contamination to a great extent. Although the corresponding EDS mapping confirms the presence of very small amounts of Sn and I elements [Fig. S4], these ribbons own high purity in spite of the participation of mineralizers (Sn and I) in the preparation process.
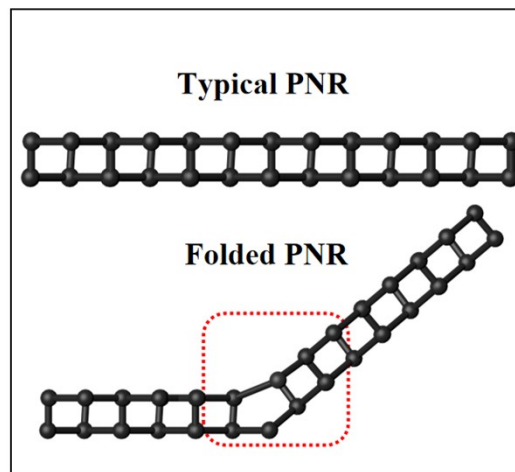

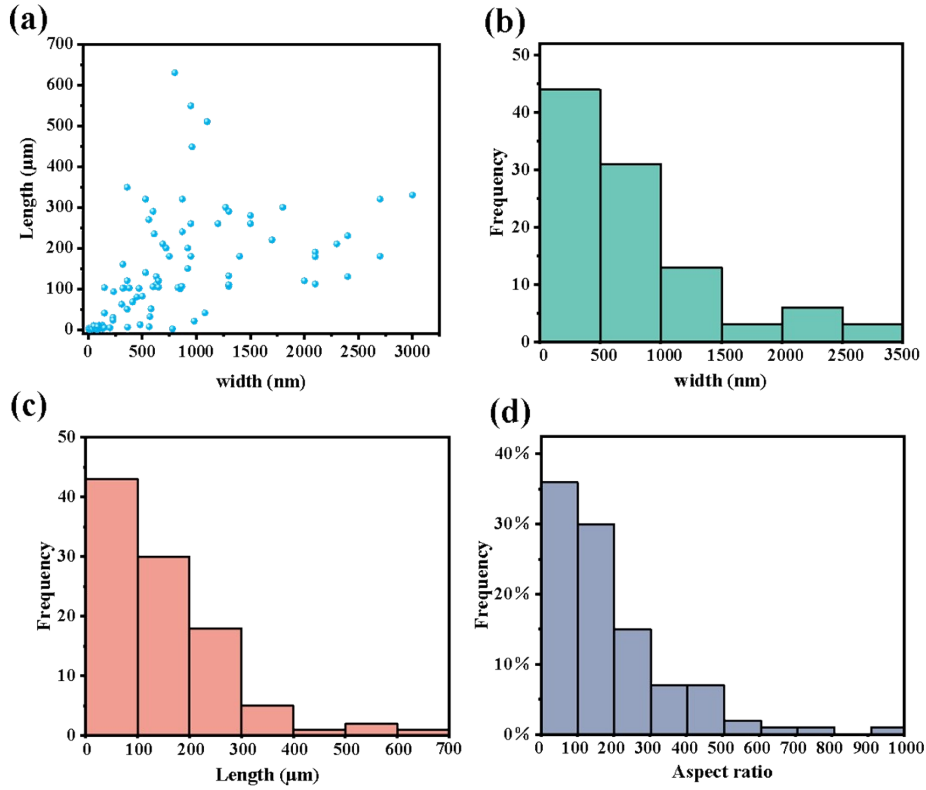FIG. S5. A schematic of lattice dislocations, corresponding to the bent PNR in FIG. 2(d).

FIG. S6. (a) The scatterplot of the length of PNRs as a function of the width for 100 PNRs and the corresponding frequency histograms for (b) length, (c) width, and (d) aspect ratio.

From the above microscope data, the length and width of one hundred PNRs were measured and plotted as a scatterplot in Fig. 3(d). The width of these PNRs ranges from ~10 nm to 3 μm, while the length range covers roughly from 2 to 640 μm. Over half of the PNRs are more than 100 μm in length, and most of the PNRs are below 1 μm in width [Fig. 3(e,f)]. Moreover, the length-to-width aspect ratios of ~65% PNRs are over 100, showing the quasi-one-dimensional characteristic [Fig. 3(g)]. In particular, ultra-long PNR with aspect ratio of ~1000 can be obtained when the width is greater than 500 nm.
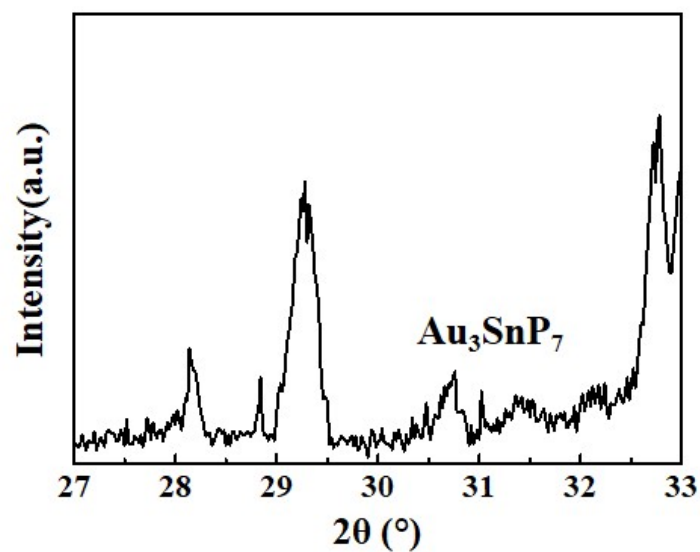
FIG. S7. Enlarged XRD pattern of as-grow PNRs in FIG. 3(b), showing the presence of trace Au_3SnP_7.

When cooling to ~485 °C, P reacted with Sn and Au forming Au_3SnP_7 on silicon, which plays a vital role in the nucleation of phosphorene. So, a crucial temperature that affects the phase transition is 485 °C, and the holding time at this stage needs to be more than 3 h. Too lower or higher temperature will lead to the final product of white P mixed with RP.
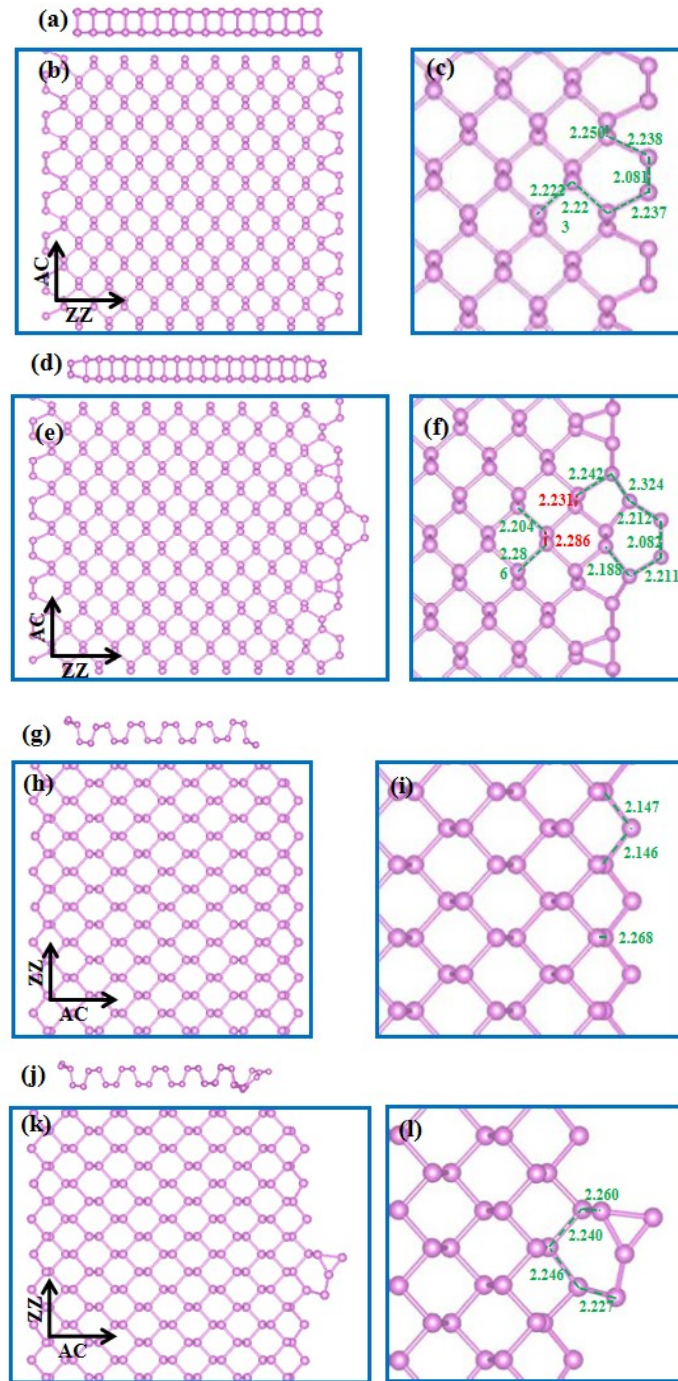
FIG. S8. The PNRs growth along ZZ direction: (a) Side and (b) top views of the initial state, and (c) the top view with partial bond lengths; (d) Side and (e) top views of the final state of PNRs and (f) the view with partial bond lengths. The PNRs growth along AC direction: (g) Side and (h) top views of the initial state and (i) the top view with partial bond lengths; (j) Side and (k) top views of the final state of PNRs and (l) the view with partial bond lengths.
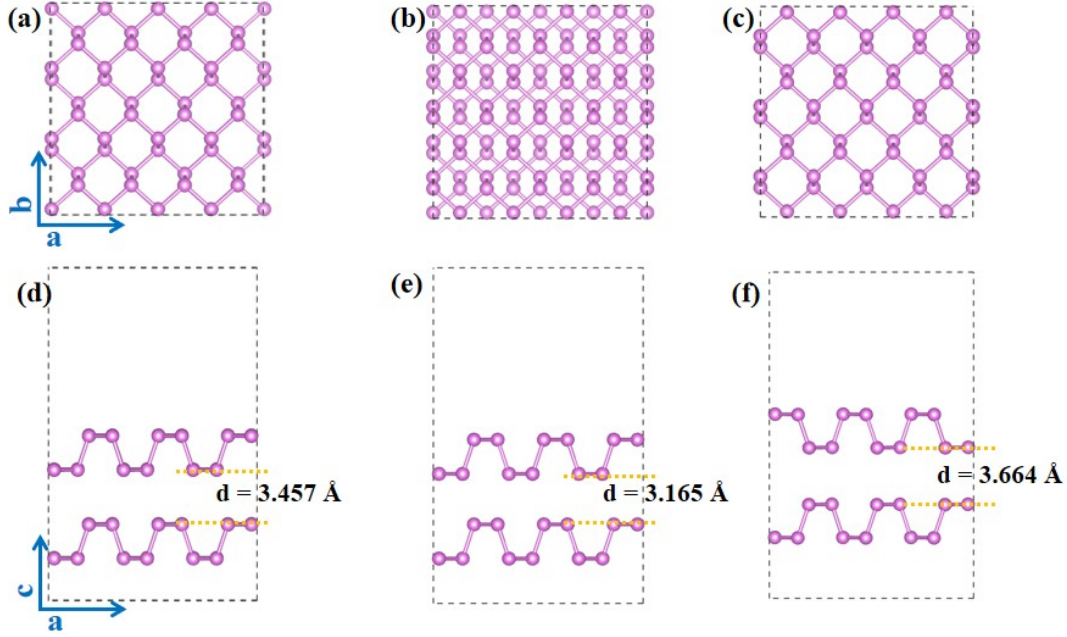
FIG. S9. Three stacking structures of bilayer phosphorene: (a–c) Top and (d–f) side views of AA-, AB-, and AC-stacking, respectively.

Three possible stacking orders of bilayer phosphorene are considered, namely, AA-, AB-, and AC-stacking [Fig. S9]. As shown in Fig. S9(a), the top layer is directly stacked on the bottom layer for the AA-stacking. The AB-stacking can be viewed as shifting the bottom layer of the AA-stacking by half of the cell along a or b direction [Fig. S9(b)]. As a result, the edge of the puckered hexagon of the top layer is located in the center of the puckered hexagon of the bottom layer. For the AC-stacking, the top and bottom layers are mirror images of each other [Fig. S9(c)]. The most notable difference among the three stacking orders is the nearest distance between the top and bottom layer, which varies from 3.165 Å of the AB-stacking to 3.664 Å of the AC-stacking [Fig. S9(d–f)]. Our total energy calculations indicate that the AB-stacking is the most stable. Assuming that the AB-stacked bilayer possesses the relative energy of 0 eV, the relative energys are 0.426 and 0.903 eV for the AA- and AC-stacked bilayers, respectively. For AB, AA and AC-stacking, as interlayer spacing increase, the relative energy increase, the stability of the structure is reduced.
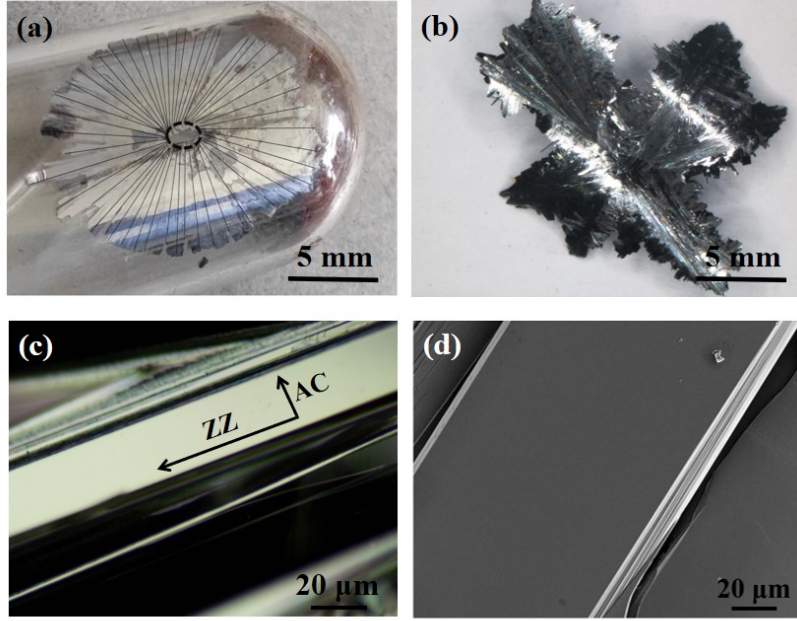
FIG. S10. As-obtained bulk BP under the absence of space confinement: (a) Representative image of BP sample in a quartz ampule tube; (b) Typical OM image of bulk BP; (c) OM and (d) SEM images of BP crystal laths.

Supplementary Note

The steady gas transport favors the preferred growth of homogeneous PNRs, which depends on the tube structure from the Reynolds coefficient[9]

$$\text{Re} = \rho v D / \gamma \qquad \text{Eq. S2}$$

where D, ρ, v and γ denote the tube diameter, gas density, gas flow rate and coefficient of viscosity. Here we used two quartz half-cylinders to obtain a smaller Reynolds coefficient for a more steady gas transport on the silicon surface.

Within the quasi-stationary boundary condition, the concentration of P_4 on the surface of PNRs will be governed by the common 2D diffusion equation[10]

$$D_c \nabla^2 C - gC + d = 0 \qquad \text{Eq. S3}$$

where Dc, C, g and d is the diffusion constant, local P_4 concentration, phosphorus consuming rate due to growth and phosphorus deposition rate, respectively. Obviously, the d on the surface will reduce when the system possesses a lower C.

References

1. G. Kresse and J. Furthmuller, *Phys. Rev. B*, 1996, **54**, 11169–11186.

2. Y. Wang, P. J. Zuo, S. B. Ma, B. X. Xie, Z. J. Yu, and G. P. Yin, *Chem. Commun.*, 2020, **56**, 12857–12860.

3. J. P. Perdew, K. Burke, and M. Ernzerhof, *Phys. Rev. Lett.,* 1996, **77**, 3865–3868.

4. G. Kresse and D. Joubert, *Phys. Rev. B*, 1999, **59**, 1758–1775.

5. S. Grimme, J. Antony, S. Ehrlich, H. Krieg, *J. Chem. Phys.,* 2010, **132** , 154104.

6. M. Y. Wang, R. F. Song, Q. Zhang, C. Li, Z. Xu, G. Liu, N. Wan, and S. Lei, *Fuel,* 2022, **321**, 124101.

7. H. Yang, Y. Wu, G. Li, Q.Lin, Q Hu, Q. Zhang, J. Liu, and C. He, *J. Am. Chem. Soc.,* 2019, **141**,12717–12723.

8. M. Y. Wang, H. Shi, M. Tian, R. W. Chen, J. P. Shu, Q. Zhang, Y. H. Wang, C. Y. Li, N. Wan, and S. Y. Lei, *ACS Appl. Nano Mater.,* 2021, **321**, 124101.

9. C. Y. Yan, L. Gan, X. Zhou, J. Guo, W. J. Huang, J. W. Huang, B. Jin, J. Xiong, T. Y. Zhai, and Y. R. Li, *Adv. Funct. Mater.,* 2017, **27**, 1702918.

10. J. Zhao, M. Shaygan, J. Eckert, M. Meyyappan, and M. H. Rummeli, *Nano Lett.,* 2014, **14**, 3064–3071.